

# The efficiency of passive confinement in CFT columns

Mathias Johansson†

*Department of Structural Engineering, Concrete Structures, Chalmers University of Technology,  
SE-412 96 Göteborg, Sweden*

(Received February 4, 2002, Accepted August 16, 2002)

**Abstract.** The paper describes the mechanical behavior of short concrete-filled steel tube (CFT) columns with circular section. The efficiency of the steel tube in confining the concrete core depending on concrete strength and the steel tube thickness was examined. Fifteen columns were tested to failure under concentric axial loading. Furthermore, a mechanical model based on the interaction between the concrete core and the steel tube was developed. The model employs a volumetric strain history for the concrete, characterized by the level of applied confining stress. The situation of passive confinement is accounted for by an incremental procedure, which continuously updates the confining stress. The post-yield behavior of the columns is greatly influenced by the confinement level and is related to the efficiency of the steel tube in confining the concrete core. It is possible to classify the post-yield behavior into three categories: strain softening, perfectly plastic and strain hardening behavior. The softening behavior, which is due to a shear plane failure in the concrete core, was found for some of the CFT columns with high-strength concrete. Nevertheless, with a CFT column, it is possible to use high-strength concrete to obtain higher load resistance and still achieve a good ductile behavior.

**Key words:** concrete-filled steel tubes; confined concrete; passive confinement; high-strength concrete; mechanical model; experiments.

## 1. Introduction

One of the most important design considerations for ductility in reinforced concrete columns is the provision of sufficient transverse reinforcement in order to confine the compressed concrete; see Mander *et al.* (1988), Cusson and Paultre (1995), Claeson (1998), and Razvi and Saatcioglu (1999). The restraint action by the lateral reinforcement prevents the concrete from cracking and failing in a brittle way, which gives higher load resistance and deformation capacity to the concrete. Furthermore, Claeson (1998) found that the spacing of the stirrups and the reinforcement configuration are of the greatest importance for the post-peak behavior, especially for high-strength concrete (HSC) columns. It has been shown that concrete-filled steel tube (CFT) columns offer a very competitive solution to the conventional reinforced concrete columns, since the steel tube confines the entire concrete core; see Bergman *et al.* (1995). This is particularly noticeable for CFT columns with circular section, where the restraint action provided by the steel tube induces uniform confining pressure to the concrete core.

For conventional reinforced concrete columns it is not only possible, but also necessary, to design the axial and lateral reinforcement as separate parts. However, in a CFT column where the steel tube is used both to take axial load and to confine the concrete core, the axial and lateral stresses interact and cannot

†M.Sc. and Lic.Sc., Research Assistant

easily be separated. The confining pressure provided by the steel tube is not constant, as in the case of active confinement, and it is not so easily measurable. The former is known as passive confinement and it depends on the difference in dilatation characteristics of the concrete and the steel, as well as on the present stress state in the steel tube. Consequently, when the concrete core is confined by a steel tube and subjected to compression, its nonlinear behavior cannot be represented by the unconfined case or the actively confined case. Furthermore, earlier results indicate that concrete with a higher unconfined compressive strength exhibits smaller confinement effects than lower-strength concrete; see Bridge and O'Shea (1999) and Shams and Saadeghvaziri (1999). This is because, with increased compressive strength, the stiffness also increases, resulting in less lateral expansion required to mobilize the restraint offered by the steel tube. Thus, the concrete experiences less confining pressure, which affects the resistance and deformation capacity of the CFT column.

From the discussion above, it is obvious that the key issue in understanding the mechanical behavior of short CFT columns is the interaction between the concrete core and the steel tube. The purpose of this study was to examine the mechanical behavior of short CFT columns with circular section, subjected to concentric compression, and to investigate the efficiency of the steel tube in confining the concrete core depending on the steel tube thickness. Of special interest was the use of HSC. Furthermore, a mechanical model based on the interaction between the concrete core and the steel tube was developed.

Several analytical models concerning the load-deformation relationship for short CFT columns can be found in the literature: Shams and Saadeghvaziri (1999), Sun and Sakino (2000) and Han *et al.* (2001). Although they show good agreement with experimental results, they are all more or less empirical. More sophisticated analytical models for similar problems have been proposed; Ahmad and Shah (1982) developed a model for concrete confined by spiral reinforcement, and Madas and Elnashai (1992) a model for different configuration of transverse reinforcement. Both these models are based on constitutive relations for the hoop reinforcement and the plain concrete subjected to active confinement. The real situation of passive confinement is accounted for by an incremental procedure, which continuously updates the confinement stress. The proposed model in this study is mainly based on the same philosophy, with the important extensions that the concrete dilatation is based on a volumetric strain history characterized by the level of applied confining stress and that it takes into account the biaxial stress state in the steel tube.

The first section of this paper describes the experimental part of the study including test set-up, material properties and results. Next, a detailed description of the proposed mechanical model is given. This is followed by a discussion of the results, including a calibration of the model against the experimental results. Finally, some remarks and conclusions are presented.

## 2. Experiments

### 2.1. Design of the tests

The tests consisted of 15 short columns tested to failure under concentric axial loading. Twelve of these columns were circular hollow steel sections filled with concrete and three were unfilled steel tubes. The latter three were to be used as reference columns. The lengths of the columns,  $l_c$ , were 650 mm with circular 159 mm diameter cross sections. The parameters varied in the experimental study were:

- two concrete grades, C30 and C85;
- three different thicknesses of the steel tube, 5.0, 6.8 and 10.0 mm;

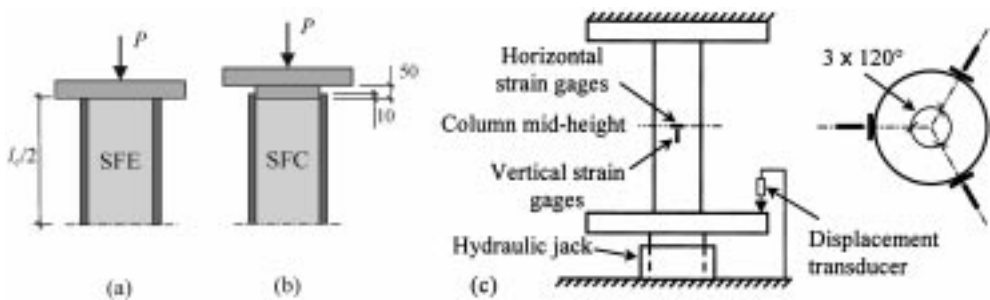


Fig. 1 Load applied to (a) the entire section, (b) to the concrete section, and (c) instrumentation of the columns

- two means of load application, the entire section (a) or the concrete section (b); see Fig. 1.

The test program is presented in Table 1. The table also includes information and results from the experiments conducted in Johansson (2000).

The material properties of the concrete at the age of 28 days are given in Table 2. The compressive cylinder strength,  $f_{c,cyl}$ , and the modulus of elasticity,  $E_0$  and  $E_c$ , refer to tests on cylinders ( $\varnothing 150 \times 300$  mm). The compressive cube strength,  $f_{c,cube}$ , refers to test cubes ( $150 \times 150 \times 150$  mm). The fracture energy,  $G_F$ , is obtained from three-point bending tests according to RILEM. The yield strength  $f_y$ , ultimate strength  $f_u$ , strain at yielding  $\varepsilon_{ay}$ , strain at hardening  $\varepsilon_{ah}$ , ultimate strain  $\varepsilon_{au}$  and modulus of elasticity  $E_a$  of the steel are given in Table 3. The material values given are the average values from three tensile tests.

The tests were carried out in a vertical hydraulic testing machine. The load was evaluated with measurements from an oil pressure gage and was increased manually at a constant rate up to maximum load. The vertical displacement of the lower, movable loading plate of the column-testing machine was measured in relation to the laboratory floor. Except for the empty reference columns, three vertical and three horizontal strain gages, arranged 120° apart, were attached to the columns at mid-height. The load arrangement and instrumentation can be seen in Fig. 1. For further details about the experimental study see Demarchi (2000).

## 2.2. Test results

The structural behaviors of specimens are represented in Fig. 2 by relations between the load,  $P$ , and the vertical deformation,  $\delta$ . The load-deformation curves obtained from the tests can be classified into three types: type 1 (a or b), type 2 and type 3 (a or b), which are schematically shown in Fig. 3.

The response of type 1 schematically represents the behavior of columns SFE 7, SFE 8, SFC 7 and SFC 8, showing a softening branch after the peak load. In particular, for columns SFE 8 and SFC 8 the softening branch after the maximum load has a low inclination until large vertical deformations (response type 1b). Columns SFE 7 and SFC 7 show a clear drop in the total axial load after the maximum load is reached, followed by a horizontal plateau (response type 1a). In this case, the values of the yielding load and the ultimate load are quite close and they can be considered equal ( $P_y \approx P_u$ ).

On the contrary, in the response curves of type 2 (SFE 9 and SFC 9) a long plateau can be observed after the column reaches yielding, and the same maximum load resistance is maintained until large values of the longitudinal deformations are obtained. Hence, the maximum load  $P_u$  and the yielding load  $P_y$  have values that do not differ very much. This behavior can be defined as almost linear-elastic/perfectly-plastic behavior. Also the response curves of SFE 1, SFE 2, SFE 3, SFC 1, SFC 2 and SFC 3, can be referred to this category; see Johansson (2000).

In particular, the third shape (type 3) of the response curves is characterized by strain hardening, after

Table 1 Test program and results for the columns

Column	$f_{c,cyl}$ [MPa]	$t$ [mm]	$f_y$ [MPa]	$\theta$	$P_y$ [kN]	$P_u$ [kN]	$P_y / P_{y,SES}^{2)}$	$P_u / P_{u,SES}^{3)}$	$P_y / P_{y,cal}$	$P_u / P_{u,cal}$	HI
SES 1 <sup>1)</sup>	-	4.8	433	-	910	930	-	-	-	-	-
SES 2 <sup>1)</sup>	-	4.8	433	-	930	950	-	-	-	-	-
SES 3 <sup>1)</sup>	-	4.8	433	-	940	960	-	-	-	-	-
SES 4 <sup>1)</sup>	-	4.8	433	-	900	930	-	-	-	-	-
Average	-	-	-	-	920 <sup>4)</sup>	940 <sup>5)</sup>	-	-	-	-	-
SES 5	-	5.0	390	-	890	1100	-	-	-	-	-
SES 6	-	6.8	402	-	1320	1770	-	-	-	-	-
SES 7	-	10.0	355	-	1550	2410	-	-	-	-	-
SFE 1 <sup>1)</sup>	64.5	4.8	433	0.89	2170	2180	2.38	2.31	1.01	0.90	0.95
SFE 2 <sup>1)</sup>	64.5	4.8	433	0.89	2140	2170	2.35	2.31	1.00	0.89	0.96
SFE 3 <sup>1)</sup>	64.5	4.8	433	0.89	2150	2190	2.36	2.33	1.01	0.90	0.97
SFE 4	36.6	5.0	390	1.48	1550	2040	1.74	1.85	0.98	1.08	1.19
SFE 5	36.6	6.8	402	2.15	1960	2860	1.48	1.62	1.02	1.23	1.21
SFE 6	36.6	10.0	355	3.00	2100	3410	1.35	1.41	0.95	1.26	1.32
SFE 7	93.8	5.0	390	0.58	2740	2740	3.08	2.49	1.06	0.97	0.82
SFE 8	93.8	6.8	402	0.84	3220	3220	2.44	1.89	1.12	1.00	0.94
SFE 9	93.8	10.0	355	1.17	3350	3710	2.16	1.54	1.09	1.05	1.07
SFC 1 <sup>1)</sup>	64.5	4.8	433	0.89	2210	2210	2.43	2.35	1.03	0.91	1.00
SFC 2 <sup>1)</sup>	64.5	4.8	433	0.89	2210	2210	2.43	2.35	1.03	0.91	0.99
SFC 3 <sup>1)</sup>	64.5	4.8	433	0.89	2240	2250	2.46	2.39	1.05	0.92	1.01
SFC 4	36.6	5.0	390	1.48	1620	2120	1.82	1.97	1.02	1.12	1.27
SFC 5	36.6	6.8	402	2.15	2050	2830	1.55	1.60	1.07	1.22	1.30
SFC 6	36.6	10.0	355	3.00	2300	3400	1.48	1.41	1.04	1.25	1.41
SFC 7	93.8	5.0	390	0.58	2970	2979	3.34	2.71	1.15	1.05	0.87
SFC 8	93.8	6.8	402	0.84	3410	3410	2.58	1.93	1.19	1.06	0.97
SFC 9	93.8	10.0	355	1.17	3400	3820	2.19	1.59	1.10	1.09	1.10

1) Johansson (2000).

2)  $P_{y,SES}$  from the empty steel tube with corresponding tube thickness.3)  $P_{u,SES}$  from the empty steel tube with corresponding tube thickness.4) Used as  $P_{y,SES}$  for the steel with tube thickness 4.8 mm.5) Used as  $P_{u,SES}$  for the steel with tube thickness 4.8 mm.

Table 2 Material properties of the concrete at the age of 28 days

Concrete grade	$f_{c,cube}$ [MPa]	$f_{c,cyl}$ [MPa]	$E_0$ [GPa]	$E_c$ [GPa]	$G_F$ [N/m]
C30	52.3	36.6	32.6	31.8	116
C55 <sup>1)</sup>	79.4	64.5	39.5	38.5	157
C85	117.2	93.8	45.9	45.3	148

1) Johansson (2000).

Table 3 Material properties of the steel

$t$ [mm]	$f_y$ [MPa]	$f_u$ [MPa]	$\varepsilon_{ay}$ [%]	$\varepsilon_{ah}$ [%]	$\varepsilon_{au}$ [%]	$E_a$ [GPa]
4.8 <sup>1)</sup>	433	568	2.1	29	136	206
5.0	390	551	2.0	13	110	193
6.8	402	603	2.0	13	199	199
10.0	355	542	1.8	13	115	203

1) Johansson (2000).

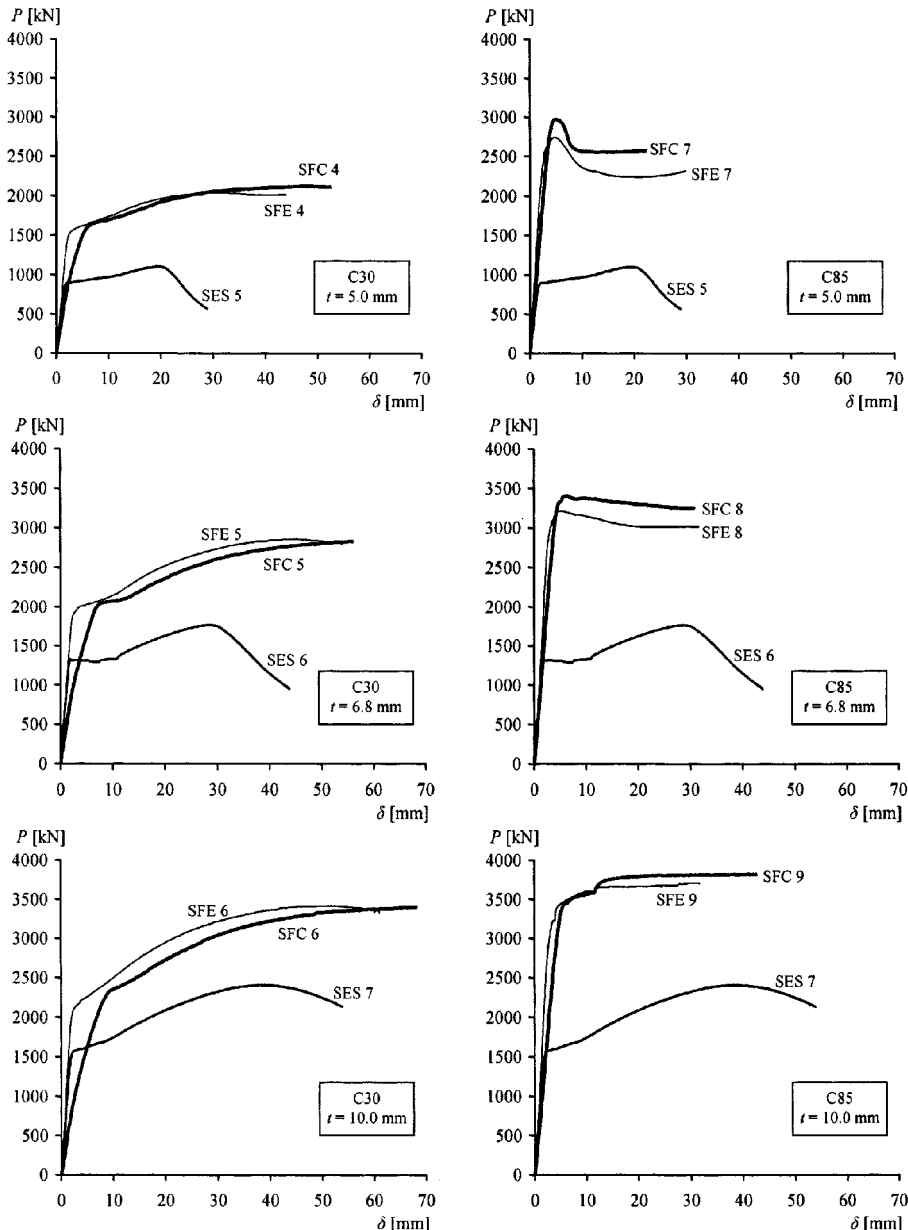


Fig. 2 Measured load versus vertical deformation

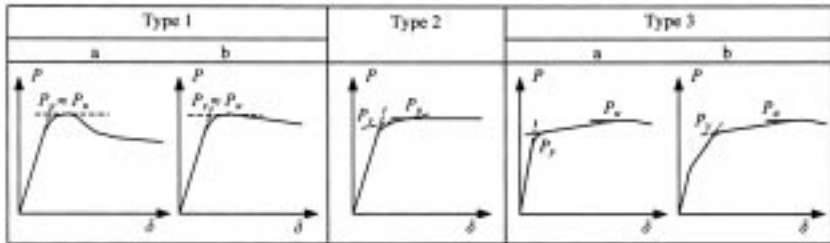


Fig. 3 Classification of the load-deformation behavior obtained in the experiments

the yielding load has been reached; in other words, the axial load carried by the columns continues to increase after yielding. This is specifically the case of columns SFE 4, SFE 5, SFE 6, SFC 4, SFC 5 and SFC 6. It is possible to observe that the curves of type 3 actually show a slightly different shape at the beginning, in the elastic range. In fact, the response of columns SFE 4, SFE 5 and SFE 6 is linear elastic until the yielding load is reached, indicated as  $P_y$ , as schematically represented in Fig. 3 (type 3a). However, the response curve of columns SFC 4, SFC 5 and SFC 6 shows a first small deviation from the initial linearity before the yielding load  $P_y$  (type 3b). The ultimate load  $P_u$ , for columns with a load-deformation curve represented by type 3, is then much higher than the yielding load,  $P_y$ , and it is reached for high value of vertical deformations.

A similar classification of load-vertical deformation curves obtained from experimental studies has been proposed by Tomii *et al.* (1977). In that case it was shown that the sectional shape of the axially loaded composite columns, in combination with the varied concrete strength and the steel tube thickness, was influencing the shape of the load-deformation curves. In particular, for certain values of the concrete strength and the steel tube thickness, the response curves of the square columns were found to follow the outline of curve type 1. But the corresponding curves of the circular columns could be classified as curve type 3. It seems reasonable to believe that this behavior is a result of the reduced confinement efficiency in the columns with square sections. However, the same reduced "confinement efficiency" can be observed in the load-vertical deformation curves obtained in this experimental study, when in general thinner steel tubes are used in combination with concrete with a higher strength.

A general observation of the structural behavior of the CFT columns seems to suggest a relation with both the concrete strength and the steel tube thickness. Therefore a ratio used by Cai *et al.* (1996) and defined as the "confinement index",  $\theta$ , is introduced; see Eq. (1). The values of  $f_y$  and  $f_{c,cyl}$  are both taken from the material tests; see Tables 2 and 3. The section areas of the steel and concrete are  $A_a$  and  $A_c$ , respectively. To quantify the post-yield behavior of the column, a hardening index,  $HI$ , is also introduced. It is defined as the load at five times the yield strain,  $P_{5\epsilon_y}$ , divided by the yielding load,  $P_y$ ; see Eq. (2).

$$\theta = \frac{A_a f_y}{A_c f_{c,cyl}} \quad (1)$$

$$HI = \frac{P_{5\epsilon_y}}{P_y} \quad (2)$$

This means that  $HI < 1$  represents a strain softening behavior (type 1 curve),  $HI = 1$  represents perfectly plastic behavior (type 2 curve) and  $HI > 1$  represents a strain hardening behavior (type 3 curve). It can be noted that for confinement index larger than approximately 1.0, hardening can be

expected and, most importantly, for confinement index lower than approximately 1.0 a softening behavior can be expected; see Fig. 4b. The further below 1.0 the confinement index is, the more pronounced is the drop in load resistance.

The different ways of load application (load on entire section or only on concrete core) do not seem to significantly change the shapes of the response curves, but only the values of the yielding and maximum loads and of the vertical deformations. In fact, only in the case of the tubes filled with normal-strength concrete, the shape of the curve is of type 3a when the entire section is loaded, and of type 3b when the load is applied only to the concrete core. However, it can be easily observed that the initial stiffness of the composite columns increases when the entire section is loaded and the steel directly contributes to carrying axial load, compared to the case of the load applied to the concrete core. This effect is very evident when the steel tube is filled with normal-strength concrete (NSC). The yielding loads,  $P_y$ , and ultimate loads,  $P_u$ , given in Table 1 are evaluated according to the definition in Fig. 3. The yielding loads obtained from the tests are compared with the yielding load,  $P_{y,cal}$ , of the composite column, calculated by assuming that the steel yields in the axial direction when the concrete fails and the circumferential steel stress is equal to zero:

$$P_{y,cal} = f_{c,cyl} A_c + f_y A_a \quad (3)$$

It is possible to observe that the squash load is a rather good estimation of the "yielding" load of the columns filled with concrete C30 and C55 (Table 1). However, for the C85 concrete-filled tubes, the squash load slightly underestimates the yield resistance. According to Eurocode 4 (1992) the ultimate load resistance,  $P_{u,cal}$ , for a short CFT column under axial compression is calculated as:

$$P_{u,cal} = A_a \eta_2 f_y + A_c [1 + \eta_1(t/D)(f_y/f_{c,cyl})] f_{c,cyl} \quad (4)$$

This expression includes the effects of confinement; the term  $\eta_2$  can be considered the steel reduction factor that reduces the steel axial compressive strength due to the circumferential tension in the steel tube. Furthermore, the expression  $[1 + \eta_1(t/D)(f_y/f_{c,cyl})]$  can be considered as the concrete enhancement factor that increases the unconfined concrete strength. The ultimate load resistance is in good agreement with the experimental results for columns filled with concrete C85, but for concrete C30 and C55 the resistances are underestimated and overestimated, respectively; see Table 1. However, this is

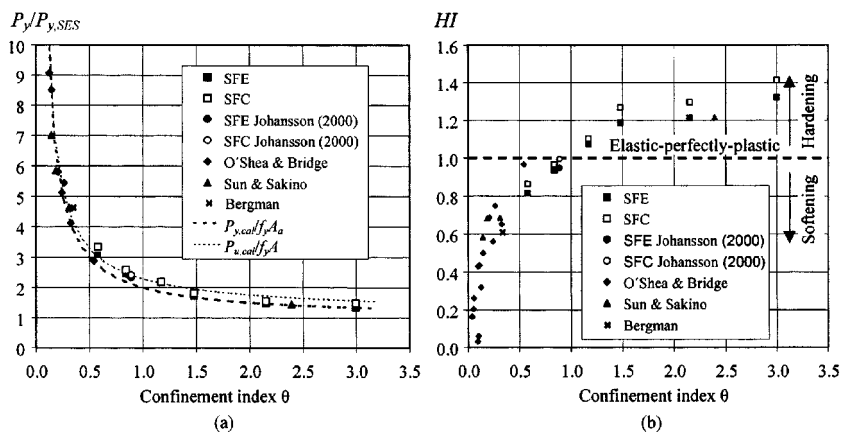


Fig. 4 (a) The efficiency of filling the steel tube with concrete and (b) the post-yield behavior of the column

probably explained by the strain hardening in the steel, rather than the accuracy of Eq. (4).

In Fig. 4a the yielding load,  $P_y$ , of the columns is normalized with respect to the yielding load of the empty steel tubes,  $P_{y,SES}$ . It is quite obvious, and also not surprising, that the efficiency of filling the steel tube with concrete increases rapidly for lower values of the confinement index. Consequently it is very advantageous, in terms of load resistance, to fill thinner steel tubes with HSC. However, for lower values of confinement index the ductility of the column decreases very fast; see Fig. 4b. Han *et al.* (2001) made the same observations for square-section columns. A comparison can also be made to results from tests on CFT columns with lower confinement index, performed by Bergman (1994) and O'Shea and Bridge (1997), and with higher confinement index performed by Sun and Sakino (2000).

### 3. Passive confinement model for short CFT columns

#### 3.1. Fundamental behavior of short CFT columns

The mechanical behavior of short concrete-filled steel tubes concentrically loaded on the entire section ( $\varepsilon_{al} = \varepsilon_c = \varepsilon_v$ ) is significantly affected by the difference in dilatation characteristics of the two materials (Poisson's effect); see Gardner and Jacobson (1967). If the steel tube and the concrete core were able to expand freely, they would experience the lateral strains  $\varepsilon_{ahf} = -V_a \varepsilon_v$  and  $\varepsilon_{chf} = -V_c \varepsilon_v$ , respectively; see Fig. 5a. In the initial stage of loading, the expansion of the concrete is smaller than for the steel ( $\varepsilon_{chf} < \varepsilon_{ahf}$ ); therefore, the steel tube expands faster in the radial direction than the concrete core, i.e., the steel does not restrain the concrete core. As the load increases and the compressed concrete starts to plasticize, the free lateral deformations of the concrete become larger than those of the steel ( $\varepsilon_{chf} > \varepsilon_{ahf}$ ). However, since strain compatibility,  $\varepsilon_{ah} = \varepsilon_{ch}$ , has to be achieved, the steel tube and the concrete core have to expand and contract, respectively. Thus, the final lateral strains in the steel and the concrete can be expressed by Eqs. (5a) and (5b), respectively:

$$\varepsilon_{ah} = \varepsilon_{ahf} + \varepsilon_{ahr} = -V_a \varepsilon_v + \varepsilon_{ahr} \quad (5a)$$

$$\varepsilon_{ch} = \varepsilon_{chf} - \varepsilon_{chr} = -V_c \varepsilon_v - \varepsilon_{chr} \quad (5b)$$

Horizontal force equilibrium for the free body diagram in Fig. 5b and the assumption of elastic materials give:

$$2r\sigma_{ch} = 2t\sigma_{ah} \Rightarrow 2r\varepsilon_{chr}E_c = 2t\varepsilon_{ahr}E_a \quad (6)$$

Using the condition of strain compatibility, together with Eqs. (5) and (6), the restrained steel strain

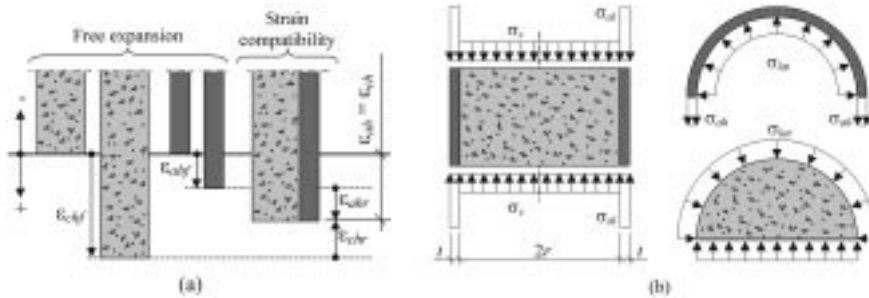


Fig. 5 (a) Lateral strain compatibility and (b) stress condition in the CFT column

can be expressed as:

$$\varepsilon_{ahr} = \frac{\varepsilon_v(v_a - v_c)}{\left(1 + \frac{tE_a}{rE_c}\right)} \text{ for } (\varepsilon_{chf} > \varepsilon_{ahf}) \quad (7)$$

From Eq. (7) it is obvious that the restrained steel strain depends on the difference in Poisson's ratio of the steel,  $v_a$ , and the concrete,  $v_c$ , i.e., the different dilatation characteristics of the two materials. For further increase in load, the steel tube restrains the concrete core and the circumferential stresses in the steel,  $\sigma_{ah}$ , become tensile and induce compressive confining pressure,  $\sigma_{lat}$ , to the concrete core. From force equilibrium, the confinement pressure is found to be a linear function of the horizontal steel stress as:

$$\sigma_{lat} = \sigma_{ah} \frac{t}{r} \quad (8)$$

At this stage and later on, the concrete core is stressed triaxially and the steel tube biaxially. As the axial strain increases, the confining pressure increases as well, and the strength and ductility of the concrete increase. Furthermore, the axial compressive resistance of the steel tube must be lower than the yield strength when circumferential steel stress is present. To calculate the total load history of the CFT column, these effects have to be taken into account. From the above discussion, it is evident that the degree of confinement is a function of the axial strain imposed; hence, the mechanical behavior can only be solved incrementally:

$$P(\varepsilon_v) = N_a(\varepsilon_v) + N_c(\varepsilon_v) = \sigma_{al}(\varepsilon_v)A_a + \sigma_c(\varepsilon_v)A_c \quad (9)$$

In the following sections the proposed model for CFT columns is described. First, the models used to describe the compressive behavior of the concrete subjected to lateral confinement are explained. Secondly, the model used to take the biaxial stress state in the steel into consideration is described. Finally, the calculating procedure of the proposed model is described.

### 3.2. Compressive behavior of concrete under lateral confinement

#### 3.2.1. Stressstrain model for concrete

It is a well-known fact that concrete experiences enhanced strength and apparent ductility under increasing lateral confinement pressure. This effect is due to the delayed damage in the microstructure due to the applied confining stress, and Imran and Pantazopoulou (1996) noted that the confined concrete strength is reached at zero volumetric strain; see Fig. 6 and Section 3.2.2. However, the behavior of confined concrete depends on several parameters, such as the uniaxial compressive strength and the level of applied confinement pressure. It has been shown that HSC does not experience the same increase in concrete strength and ductility, due to lateral confinement, as NSC. Several expressions for the confined concrete strength and corresponding strain have been proposed, among others Richart *et al.* (1928), Xie *et al.* (1995), Ansari and Li (1998), and also different stress-strain relation models for confined concrete, Mander *et al.* (1988) and Cusson and Paultre (1995). However, in this study the active confinement model proposed by Attard and Setunge (1996) has been used. This is because it is applicable for a broad range of concrete strengths and confinement pressures, which are of interest in the present study. Furthermore, it describes the softening portion of the stress-strain relationship also for larger strains. The expression for the stress-strain curve was originally proposed by Sargin (1971):

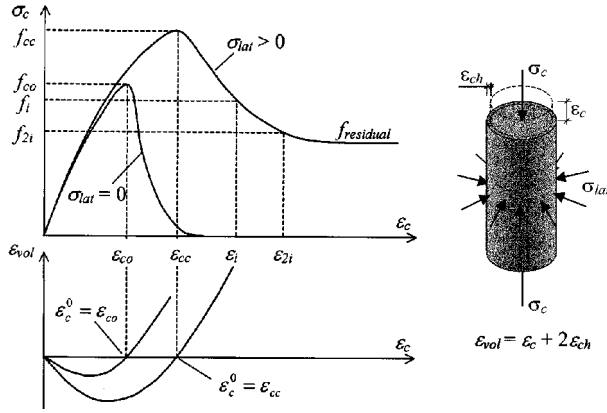


Fig. 6 The stress-strain and volumetric strain model used for confined concrete

$$Y = \frac{AX+BX^2}{1+CX+DX^2} \quad Y = \frac{\sigma_c}{f_{cc}}, \quad X = \frac{\epsilon_c}{\epsilon_{cc}} \quad \text{and} \quad \forall X \geq 0 \quad 0 \leq Y \leq 1 \quad (10)$$

where  $\sigma_c$  is the stress at strain  $\epsilon_c$ . The confined concrete strength and corresponding strain are computed as:

$$f_{cc} = f_{co} \left( \frac{\sigma_{lat}}{f_{ct}} + 1 \right)^k \quad (11)$$

$$\epsilon_{cc} = \epsilon_{co} \left[ 1 + (17 - 0.06f_{co}) \left( \frac{\sigma_{lat}}{f_{co}} \right) \right] \quad (12)$$

where  $\epsilon_{co}$  and  $f_{co}$  are determined from tests on  $\varnothing 150 \times 300$  mm cylinders,  $f_{ct}$  is the tensile strength of concrete, and  $k$  is a parameter that reflects the effectiveness of confinement and is calculated as:

$$k = 1.25 \left[ 1 + 0.062 \frac{\sigma_{lat}}{f_{co}} \right] f_{co}^{-0.21} \text{ MPa} \quad (13)$$

Two sets of the constants  $A$ ,  $B$ ,  $C$  and  $D$  are required, one for the ascending branch and a second for the descending branch. For the ascending branch,  $\epsilon_c \leq \epsilon_{cc}$ , the constants are given by:

$$A = \frac{E_c \epsilon_{cc}}{f_{cc}} \quad (14)$$

$$B = \frac{(A-1)^2}{(1 - (0.45f_{co}/f_{cc}))} \quad (15)$$

$$C = (A-2) \quad (16)$$

$$D = (B+1) \quad (17)$$

In uniaxial compression, the failure mode is a combination of tensile splitting and shear failure, which causes a steep descending branch. However, the descending branch of the stress-strain curve for confined concrete is different from that of the uniaxial case, in that it approaches a residual strength

level for large strains. The residual strength represents the load carried by friction across the cracked shear plane. To define the constants for the descending branch, two points on the descending curve are required. The coordinates for these points are denoted  $\varepsilon_i, f_i$  and  $\varepsilon_{2i}, f_{2i}$  (see Fig. 6). Expressions for these parameters can be found in Attard and Setunge (1996). For the descending branch  $\varepsilon_c \geq \varepsilon_{cc}$ , the constants  $A$  and  $B$  are given by:

$$A = \left[ \frac{\varepsilon_{2i} - \varepsilon_i}{\varepsilon_{cc}} \right] \left[ \frac{\varepsilon_{2i}(f_i/\varepsilon_i)}{(f_{cc}-f_i)} - \frac{4\varepsilon_i(f_{2i}/\varepsilon_{2i})}{(f_{cc}-f_{2i})} \right] \quad (18)$$

$$B = (\varepsilon_i - \varepsilon_{2i}) \left[ \frac{(f_i/\varepsilon_i)}{(f_{cc}-f_i)} - \frac{4(f_{2i}/\varepsilon_{2i})}{(f_{cc}-f_{2i})} \right] \quad (19)$$

while  $C$  and  $D$  are still given by Eqs. (16-17). To establish the full stress-strain relationship for confined concrete, the parameters required are therefore the unconfined compressive strength, the strain at peak stress, the elastic modulus and the confining pressure.

### 3.2.2. Volumetric strain model for concrete

Imran and Pantazopoulou (1996) performed triaxial tests on concrete cylinders and stated that the level of applied confining stress,  $\sigma_{lat}$ , characterizes the volumetric strain history of the concrete; see Fig. 6. Initially, the  $\varepsilon_{vol}$ - $\varepsilon_c$  relation appears to be linear; however, the development of microcrack-related expansion in the cross section supporting the compressive stress is manifested by progressive nonlinearity in the  $\varepsilon_{vol}$ - $\varepsilon_c$  curve. Prior to cracking, i.e.,  $\varepsilon_c < \varepsilon_c^{\lim}$ , the volumetric strain is described by the following equation:

$$\varepsilon_{vol} = (1 - 2\nu_{co}) \left( \frac{-2\sigma_{lat}}{E_c} + \varepsilon_c \right) \quad (20)$$

$$\varepsilon_c^{\lim} = \frac{-(1 - \nu_{co})}{\nu_{co}E_c} \sigma_{lat} - \frac{\varepsilon_{cr}}{\nu_{co}} \quad (21)$$

and after cracking, i.e.,  $\varepsilon_c > \varepsilon_c^{\lim}$ , the volumetric strain is described as:

$$\varepsilon_{vol} = (1 - 2\nu_{co}) \left( \frac{-2\sigma_{lat}}{E_c} + \varepsilon_c^0 \left( \frac{\varepsilon_c}{\varepsilon_c^0} - \left[ \frac{\varepsilon_c - \varepsilon_c^{\lim}}{\varepsilon_c^0 - \varepsilon_c^{\lim}} \right]^2 \right) \right) \quad (22)$$

In this equation,  $\varepsilon_c^0$  represents the axial compressive strain at the instant of zero volumetric strain, taken as  $\varepsilon_{cc}$ ; see Eq. (12). Since the restraining effect of the confining pressure is considered in the volumetric strain model, the total lateral strain of the concrete can directly be calculated as:

$$\varepsilon_{ch} = \frac{(\varepsilon_{vol} - \varepsilon_v)}{2} \quad (23)$$

### 3.3. Stresses in the steel tube

The steel stresses  $\sigma_{al}$  and  $\sigma_{ah}$  can be calculated from steel strains by using Hooke's generalized law for the case of two-dimensional plane stress, as in Crisfield (1994):

$$\sigma_{ah} = \frac{E_a}{1 - \nu_a^2} (\varepsilon_{ah} + \nu_a \varepsilon_{al}) \quad (24)$$

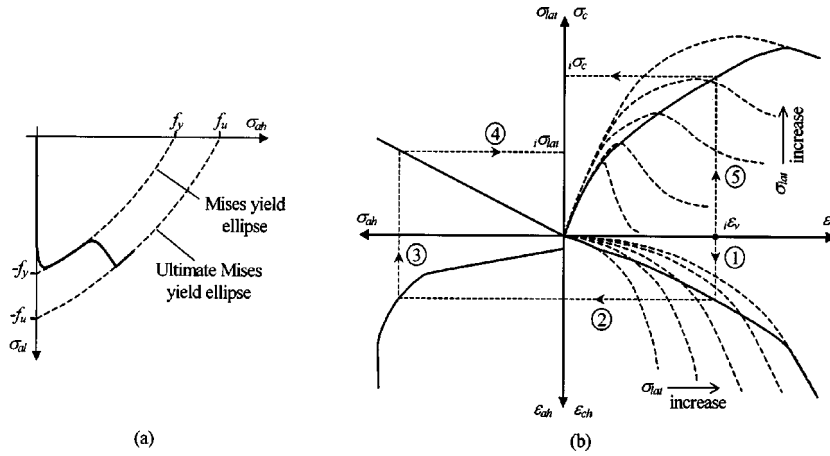


Fig. 7 (a) Stress history in the steel tube. (b) Schematic representation of the proposed model

$$\sigma_{al} = \frac{E_a}{1 - \nu_a^2} (\varepsilon_{al} + \nu_a \varepsilon_{ah}) \quad (25)$$

The Poisson's ratio  $\nu_a$  is assumed to have the initial value  $\nu_{ao}$  until half the yield strain, from where it is assumed to vary linearly up to 0.5 at yielding; see O'Shea and Bridge (1997). The stresses are limited by the simple plane stress version of the von Mises yield function (see Fig. 7a):

$$f = \sigma_e - \sigma_o = \sqrt{\sigma_{ah}^2 + \sigma_{al}^2 - \sigma_{ah}\sigma_{al}} - \sigma_o \quad (26)$$

where  $\sigma_e$  is the effective stress and  $\sigma_o$  the yield stress. Isotropic strain hardening can be introduced by changing the fixed yield stress,  $\sigma_o$ , in Eq. (26) to a variable stress,  $\sigma_o(\varepsilon_{ps})$ , so that yield stress is a function of the equivalent plastic strain; see Crisfield (1994):

$$f = \sigma_e - \sigma_o(\varepsilon_{ps}) \quad (27)$$

$$\varepsilon_{ps} = \frac{2}{\sqrt{3}} \sqrt{\varepsilon_{pal}^2 + \varepsilon_{pah}^2 + \varepsilon_{pal}\varepsilon_{pah}} \quad (28)$$

The relation between  $\sigma_o$  and  $\varepsilon_{ps}$  can be taken from the stress-plastic strain relationship for uniaxial tension.

### 3.4. Calculation procedure for the proposed model

The procedure of the uniaxial model for CFT columns is described herein. The model includes the effect of passive confinement of the concrete core and the present biaxial stress state in the steel tube. The procedure for the proposed model can be summarized in the following steps.

1. A value of axial strain,  $\varepsilon_v$ , is fixed.
2. The transverse strain,  $\varepsilon_{ch}$  ( $\varepsilon_{ah}$ ), is determined from the volumetric strain model described in Section 3.2.2.
3. The axial steel stress,  $\sigma_{al}$ , and the circumferential steel stress,  $\sigma_{ah}$ , are calculated from the strains  $\varepsilon_{al}$  and  $\varepsilon_{ah}$  (Section 3.3).

4. The confining pressure,  $\sigma_{lat}$ , is given by the linear relation in Eq. (8).
5. The concrete stress,  $\sigma_c$ , is established from the active confinement model described in Section 3.2.1.
6. The total load on the CFT column is calculated from Eq. (9).
7. Steps 1 to 6 are repeated for increasing values of  $\varepsilon_i$ , resulting in a load-deformation relationship for the CFT column.

Since the volumetric strain model has the confining pressure,  $\sigma_{lat}$ , as an input, an iteration procedure over steps 2-4 must be used. Fig. 7b depicts schematically the sequence of calculations required for the model.

## 4. Results and discussion

### 4.1. Mechanical behavior described by the proposed model

To verify the proposed model designed with emphasis on HSC, a comparison of the structural behavior, represented by load-deformation relations, obtained from the tests and that from the model was made for the specimens with concrete grade C85; see Fig. 8a. As can be seen, rather good agreement is found. The model shows a somewhat stiffer behavior than that obtained in the test. This can to some extent be explained by the fact that the recorded deformation also includes deformations in the column-testing machine, since the deformation only was measured at the lower loading plate and not between the two loading plates, which is preferable. This is especially noticeable at the beginning of the loading.

As was stated in Section 3.2, the mechanical behavior of short CFT columns loaded on the entire section is significantly affected by the difference in dilatation characteristics of the two materials. In the following, this is described for specimen SFE 7, by means of results from the proposed model.

Initially both the steel and concrete are in the elastic stage and the dilatation is equal to the initial value of Poisson's ratio,  $\nu_{ao}$  and  $\nu_{co}$  for the steel and the concrete, respectively. Since the dilatation is larger for the steel than for the concrete, they carry load independently of each other; see Figs. 8b and 9a. The steel tube experiences stresses only in the axial direction ( $\sigma_{al} > 0$ ;  $\sigma_{ah} = 0$ ) and the yield resistance is reached at point "y" for further loading; see Figs. 8b and 10b. From now on, the "free"

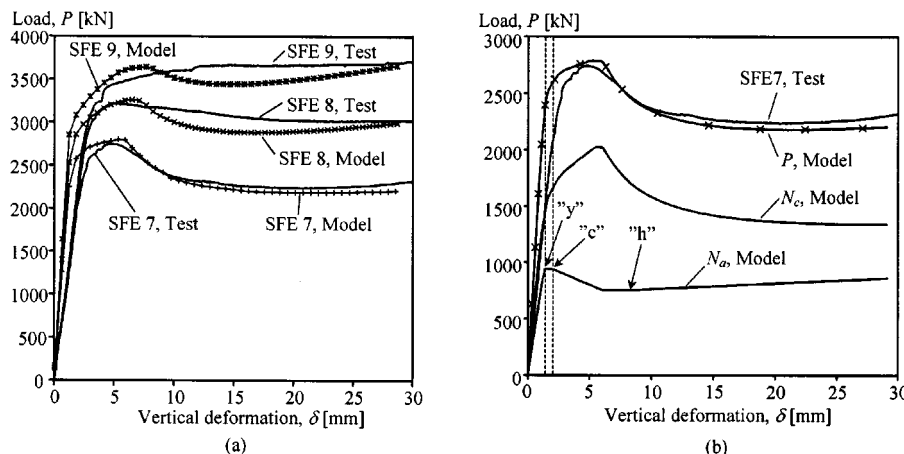


Fig. 8 (a) Comparison of load-deformation relation between experiment and proposed model. (b) Distribution of the axial load in the section of specimen SFE 7

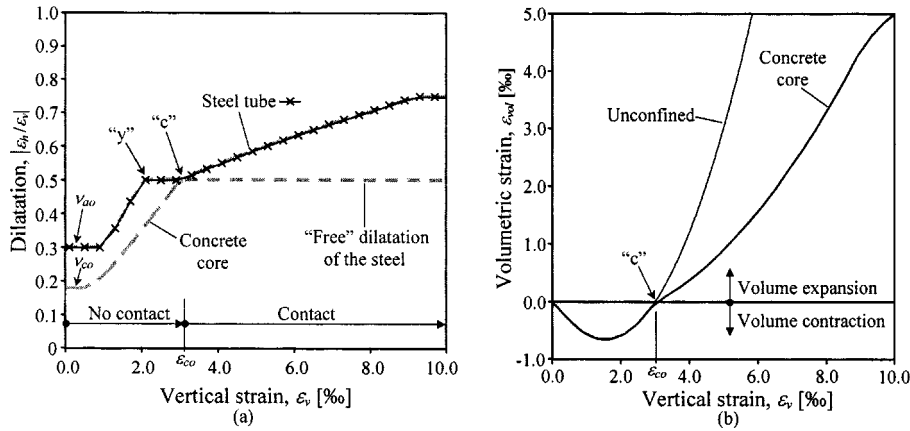


Fig. 9 (a) Dilatations and (b) volumetric strain of the concrete core (specimen SFE 7)

dilatation of the steel equals 0.5; see Fig. 9a. There is no contact between the concrete core and the steel tube before the dilatation of the concrete core becomes equal to that of the steel tube, i.e., no contact before  $|\dot{\varepsilon}_{ch}/\varepsilon_v| = 0.5$ , (denoted “c” in Fig. 9a). From Eq. (23) it can easily be found that the concrete dilatation becomes 0.5 at zero volumetric strain ( $\varepsilon_{vol}=0$ ), which occurs when the vertical strain is equal to the strain at peak stress for the unconfined case ( $\varepsilon_v=\varepsilon_{co}$ ); see Fig. 9. This means that contact occurs first when the unconfined concrete compressive strength is reached. Consequently, before this point there is no effect of confinement and the total response of the column is the sum of the responses that could be expected for the uniaxial cases of the concrete core and steel tube, respectively.

From the point where contact is obtained (“c”), the steel tube restrains the concrete core, and the steel strain and concrete strain are forced to be equal ( $\varepsilon_{ah}=\varepsilon_{ch}$ ). To achieve this, restraint strains have to develop in both the steel tube ( $\varepsilon_{ahr}>0$ ) and the concrete core ( $\varepsilon_{chr}>0$ ); see Figs. 5a and 10a. Accordingly, this means that the dilatations of the concrete core and the steel tube also must be equal; see Fig. 9a. Furthermore, the volume expansion of the core becomes smaller than for the unconfined case; see Fig. 9b. Due to further volume expansion of the concrete core, the restrained steel strains increase, which give increasing circumferential steel stress,  $\sigma_{ah}$ , and consequently also increasing

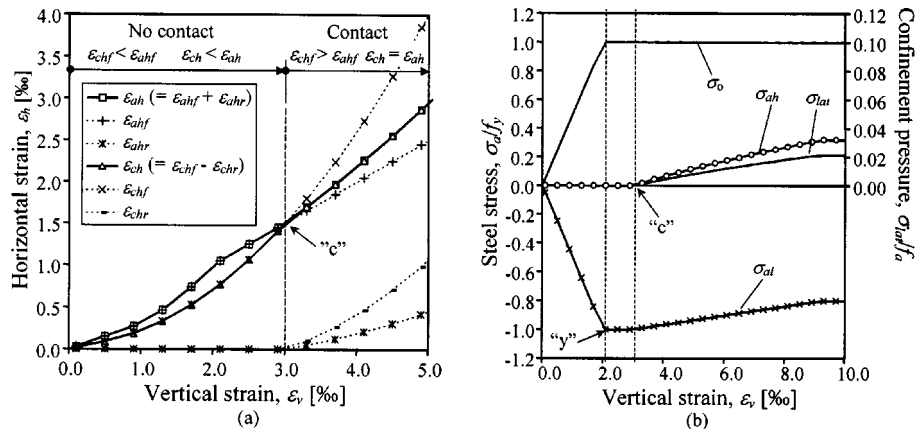


Fig. 10 (a) Lateral strains and (b) steel stresses and confinement pressure (specimen SFE 7)

contact pressure,  $\sigma_{lat}$ ; see Fig. 10b. This gives an enhanced resistance and deformation capacity of the concrete core, and the load resistance of the concrete core starts to increase. Furthermore, because of the increasing circumferential steel stress, the axial compressive stress,  $\sigma_{al}$ , in the tube decreases; see Fig. 10b.

When the dilatation starts to flatten out, the contact pressure becomes constant and the concrete will soon experience a descending branch and approaches the residual strength for the present confining pressure; see Fig. 8b. When the strain hardening for the steel is reached (denoted "h"), the total load of the column increases again -primarily due to the increase in axial steel stress, but also because of increasing confinement effects when the circumferential steel stress increases, i.e., higher confinement pressure; see Fig. 8a. These results confirm that the proposed model reflects the behavior described in Section 3.1.

#### 4.2. Influence of confinement index

From the experimental results it was found that both the load resistance and deformation capacity are influenced by the confinement index. In Fig. 11a the effect of changed confinement index is obvious. Here the diameter is kept constant and the thickness of the steel tube is varied in order to change the confinement index. It can clearly be seen that the ductility of the column decreases with lower confinement index. This is explained by the fact that, for the same lateral restrained steel strain ( $\varepsilon_{ahr}$ ) and corresponding circumferential steel stress, the resulting confinement pressure on the concrete core is lower for the thinner steel tube than for the thicker; see Eq. (8). This gives lower concrete peak and residual strengths. Furthermore, a lower confinement index means that the concrete core carries a bigger part of the total load, and consequently the response of the concrete will be more apparent.

In Fig. 11b columns with different outer diameter (159 and 210 mm) but almost the same confinement index are compared. The load resistance is, of course, higher for the larger-diameter columns; however, when the load is normalized with respect to the squash yielding load according to Eq. (3), it is obvious that the load-strain relations almost coincide for columns with similar confinement index. This strengthens the theory that the confinement index is related to the structural behavior, i.e., the shape of the load-deformation curve.

It can be noticed in Fig. 11 that the residual strength increases with higher confinement index, and in

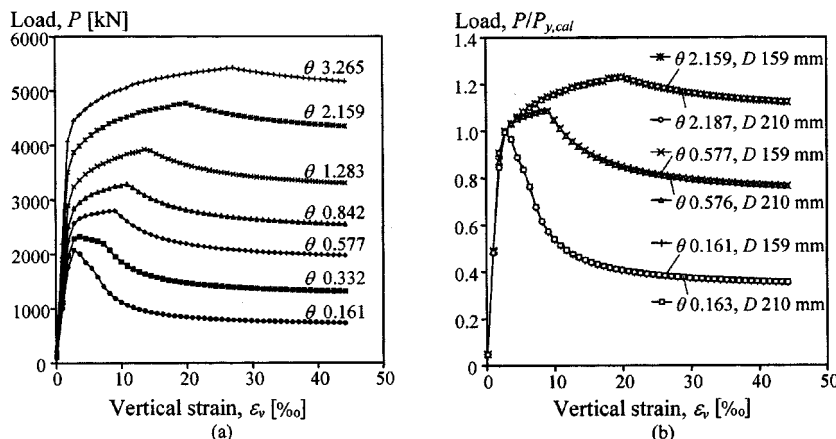


Fig. 11 (a) Load-strain relation for different confinement index,  $D = 159$  mm,  $t$  varied; (b) normalized load-strain relation,  $D = 159$  mm,  $D = 210$  mm and  $t$  varied.

the experiments even strain hardening was obtained for higher confinement index. This can of course to some extent be explained by the strain hardening of the steel tube. However, after the tests, the concrete-filled steel tubes with the smallest thickness were open and it could be observed that for SFE 4 (C30,  $\theta = 1.48$ ) the core was completely crushed, while for SFE 7 (C85,  $\theta = 0.58$ ) a clear inclined shear failure plane was visible cutting straight through the aggregates; see Demarchi (2000). Triaxial tests on concrete cylinders performed by Rutland and Wang (1997) have shown that the angle of the failure plane changes for increasing confining pressure. Moreover, Palaniswamy and Shah (1974) demonstrated the two extreme failure modes: splitting failure at low confining pressures and crushing failure at large confining pressures. In tests on rectangular HSC tied columns, Cusson and Paultre (1994) found that the failure is characterized by the formation of an inclined shear failure plane, separating the concrete core into two wedges laterally restrained by the reinforcement cage. Measured from the vertical axis, the inclination angle of the shear failure plane varied from  $25^\circ$  for lightly confined specimens to  $45^\circ$  for highly confined specimens. Further, they found that the residual strength was related to the shear plane and was low for lightly confined columns but increased with a higher amount of lateral reinforcement; see Cusson and Paultre (1995). For highly confined columns it was observed that the residual strength was equal to the peak strength of the confined concrete, indicating a ductile crushing failure typical of confined NSC. They also proposed a model to calculate the residual concrete stress corresponding to the complete formation of the shear failure plane of the reinforced concrete core. Similar observations about the formation of a shear failure plane were found for spirally reinforced HSC columns by Bjerkeli (1992).

These theories can be expected to be applicable also for CFT columns. The implication is that, with increasing confinement index, the failure of the concrete core changes from shear failure towards crushing failure and consequently, at the same time also the residual strength increases. The two extremes are, of course, zero and infinite confinement index, i.e., the unconfined case and infinite steel thickness, respectively. Furthermore, this explains why the post-peak behavior of the columns filled with the lower-strength concrete (C30), where a crushing failure was present, could not be predicted satisfactorily by the proposed model. This is because the residual strength, described by the constitutive model used for concrete, represents the load carried by friction across an inclined shear failure plane.

The observations from tests and the proposed model in this study indicate that a shear plane failure, resulting in a softening behavior, can be expected in columns with confinement index lower than approximately 1.0. For columns with confinement index exceeding approximately 1.0, a plastic or even hardening behavior could occur due to crushing failure of the concrete. The effect of changed failure mode on the post-peak behavior of the CFT column is very important to understand if an efficient use of HSC is to be possible, and it has to be further investigated.

## 5. Conclusions

The following conclusions are based on the research reported in this paper.

A mechanical model was proposed for short CFT columns with circular sections, subjected to concentric compression. The model is based on a volumetric strain history characterized by the level of applied confining stress. This comprises a procedure for calculating and continuously updating the lateral confinement stress for a given axial strain, thus accounting for the passive confinement to which the concrete core is subjected. The model was able to predict the experimental behavior for the high-strength concrete filled columns with acceptable accuracy. Furthermore, the model gives an opportunity to study the interaction between the concrete and the steel and not only the structural behavior.

It was found that for the columns with the load applied on the entire section, which is the normal loading condition assumed in design, no contact occurs between the concrete and the steel before the unconfined concrete compressive strength is reached. This means that there is no effect of confinement before this point, and the total response of the column is the sum of the responses that can be expected for the uniaxial cases of the concrete core and steel tube, respectively. However, the post-yield behavior is greatly influenced by the confinement level and is related to the efficiency of the steel tube in confining the concrete core to prevent micro cracking.

The confinement efficiency can be defined by the confinement index, and it is possible to classify the post-yield behavior from the value of the confinement index into three categories: strain softening behavior, perfectly plastic behavior and strain hardening behavior. The softening behavior is due to a shear plane failure, and can be expected in columns with confinement index lower than approximately 1.0. The more below 1.0 the confinement index is, the lower is the residual strength of the column. For confinement index larger than approximately 1.0, a plastic or even hardening behavior could occur due to crushing failure of the concrete.

It is possible to use HSC and still obtain a column with good ductile behavior when a concrete-filled steel tube is used. However, a thicker steel tube is needed for HSC compared with NSC if the same ductility is aimed at.

## Acknowledgements

The author conducted the work presented in this paper as part of his Ph.D. studies at Chalmers University of Technology. The author wishes to thank his advisors, Professor Kent Gylltoft, Head of the Department of Structural Engineering, and Christina Claeson, Ph.D., NCC AB. The author wishes to express his gratitude to the Swedish Council for Building Research (BFR) (since 2001, FORMAS), the Development Fund of the Swedish Construction Industry (SBUF) and the construction company NCC AB, for financially supporting this project.

## References

- Ahmad, S.H. and Shah, S.P. (1982), "Stress-strain curves of concrete confined by spiral reinforcement," *ACI Journal*, 79-46, 484-490.
- Ansari, F. and Li, Q. (1998), "High-strength concrete subjected to triaxial compression," *ACI Materials Journal*, 95-M75, 747-755.
- Attard, M.M. and Setunge, S. (1996), "Stress-strain relationship of confined and unconfined concrete," *ACI Materials Journal*, 93-M49, 432-442.
- Bergman, R. (1994), "Load introduction in composite columns filled with high strength concrete," *Tubular Structures VI*, Grundy, Holgate & Wong (eds.), Rotterdam, The Netherlands.
- Bergman, R., Matsui, C., Meinsma, C. and Dutta, D. (1995), *Design Guide for Concrete-Filled Hollow Section Columns under Static and Seismic Loading*, CIDECT, Verlag TÜV Rheinland GmbH, Köln, Germany.
- Bjerkeli, L. (1992), *High-Strength Concrete SP1 Beams and Columns, Report 1.1, Ductility of Spirally Reinforced Columns*, Rep. No. STF70 A92120. SINTEF Struct. Eng. FCB, Trondheim, Norway.
- Bridge, R.Q. and O'Shea, M.D. (1999), "Local buckling and confinement in axially loaded steel tubes filled with normal and high-strength concrete," *Australian Journal of Structural Engineering Transactions*, SE2(2&3), 123-133.
- Cai, S.-H. and Gu, W.-P. (1996), "Behavior and ultimate strength of steel tube confined high strength concrete

- columns," *4<sup>th</sup> Int. Symp. on Utilization of High-Strength/High-Performance Concrete*, Paris, 827-833.
- Claeson, C. (1998), *Structural Behavior of Reinforced High-Strength Concrete Columns*, Ph.D. thesis, Chalmers University of Technology, Div. of Concrete Struct., Göteborg, Sweden.
- Crisfield, M.A. (1994), *Non-linear Finite Element Analysis of Solids and Structures*, John Wiley & Sons Ltd., Chichester, England.
- Cusson, D. and Paultre, P. (1994), "High-strength concrete columns confined by rectangular ties," *J. Struct. Eng., ASCE*, **120**(3), March, 783-804.
- Cusson, D. and Paultre, P. (1995), "Stress-strain model for confined high-strength concrete," *J. Struct. Eng., ASCE*, **121**(3), March, 468-477.
- Demarchi, G. (2000), *Experimental and Analytical Study on Short Concrete Filled Steel Tubes with Circular Section*, M.Sc. Thesis, Chalmers Univ. of Techn., Dep. of Struct. Eng., Sweden.
- European Prestandard, Eurocode 4 (1992), *Design of Composite Steel and Concrete Structures, Part 1-1: General Rules and Rules for Buildings*, Ref. No.1994-1-1:1992, European Committee for Standardization, Brussels, Belgium.
- Gardner, N.J. and Jacobson, E.R. (1967), "Structural behavior of concrete filled steel tubes," *ACI Journal*, **64**(7), 404-412.
- Han, L.-H., Zhao, X.-L. and Tao, Z. (2001), "Tests and mechanics model for concrete-filled SHS stub columns, columns and beam-columns," *Steel and Composite Structures*, Techno-Press, **1**(1), March, 51-74.
- Imran, I. and Pantazopoulou, S.J. (1996), "Experimental study of plain concrete under triaxial stress," *ACI Materials Journal*, 93-M67 589-601.
- Johansson, M. (2000), *Structural Behaviour of Circular Steel-Concrete Composite Columns Non-linear Finite Element Analyses and Experiments*, Licentiate thesis, Chalmers University of Technology, Div. of Concrete Struct., Göteborg, Sweden.
- Madas, P. and Elnashai, A.S. (1992), "A new passive confinement model for the analysis of concrete structures subjected to cyclic and transient dynamic loading," *Earthquake Engineering and Structural Dynamics*, **21**, 409-431.
- Mander, J.B., Priestley, M.J.N. and Park, R. (1988), "Theoretical stress-strain model for confined concrete," *J. Struct. Eng., ASCE*, **114**(8), August, 783-804.
- O'Shea, M.D. and Bridge, R.Q. (1997), *Tests on Circular Thin-Walled Steel Tubes Filled With Medium and High Strength Concrete*, Research Report No. R755, School of Civil Engineering, University of Sydney, Australia.
- Palaniswamy, R. and Shah, S.P. (1974), "Fracture and stress-strain relationship of concrete under triaxial compression," *J. Struct. Division, ASCE*, **100**(ST5), May, 901-916.
- Razvi, S.R. and Saatcioglu, M. (1999). "Circular high-strength concrete columns under concentric compression," *ACI Struct. J.*, 96-S90, 817-825.
- Richart, F.E., Brandtzaeg, A. and Brown, R.L. (1928), *A Study of the Failure of Concrete under Combined Compressive Stresses*, Bulletin No. 185, University of Illinois, Engineering Experimental Station, Urbana, Illinois, USA, November, 104 pp.
- Rutland, C.A. and Wang, M.L. (1997), "The effects of confinement on the failure orientation in cementitious materials experimental observations," *Cement and Concrete Composites*, Elsevier Science Ltd., No. 19, 149-160.
- Sargin, M. (1971), *Stress-Strain Relationship for Concrete and the Analysis of Structural Concrete Sections, Study No. 4*, Solid Mechanics Division, University of Waterloo, Ontario, 167 pp.
- Shams, M. and Saadeghvaziri, M.A. (1999), "Nonlinear response of concrete-filled steel tubular columns under axial loading," *ACI Struct. J.*, 96-S112, 1009-1017.
- Sun, Y. and Sakino, K. (2000), "A comprehensive stress-strain model for high-strength concrete confined by circular transverse reinforcement," *Composite and Hybrid Structures, Proc. of 6<sup>th</sup> ASCCS Conf.*, Los Angeles, USA, March 22-24, 1067-1074.
- Tomii, M.Y., Yoshimura, K. and Morishita, Y. (1977), "Experimental studies on concrete filled steel tubular columns under concentric loading," *Proc. Int. Colloquium on Stability of Structures Under Static and Dynamic Loads*, 718-741.
- Xie, J., Elwi, A.E. and MacGregor, J.G. (1995), "Mechanical properties of three high-strength concretes containing silica fume," *ACI Materials Journal*, 92-M15, 135-145.